Measurement of sin2β from $B_d^0 \to J/\psi K_s^0$: statistical reach and estimate of the systematic uncertainties

Y. Coadou✪, J. Damet✪, H. Korsmo◆ and G. F. Tartarelli✻

✪ Uppsala University, Department of Radiation Sciences, Uppsala, Sweden
◆ Fysiska institutionen, Lunds universitet, Sweden
✻ Dipartimento di Fisica dell'Università di Milano e I.N.F.N., Milano, Italy

1 Introduction

The measurement of the time-dependent CP-violating asymmetry in the decay $B_d^0 \to J/\psi K_s^0$ can provide a clean measurement of the angle β of the unitarity triangle. To a very good approximation the Standard Model (SM) prediction for the asymmetry in this channel is given by:

$$A(t) = \sin 2\beta \sin(\Delta m_d t)$$

where Δm_d is the mass difference in the $B_d^0 - \overline{B_d^0}$ system. The predicted asymmetry is insensitive to the contribution from penguin diagrams. This makes the $B_d^0 \to J/\psi K_s^0$ decay the so-called *gold-plated* mode to measure the angle β. The decay $B_d^0 \to J/\psi K_s^0$, with $J/\psi \to \mu^+\mu^-$ or $J/\psi \to e^+e^-$, and $K_s^0 \to \pi^+\pi^-$, is also experimentally very clean, and data samples can be reconstructed with relatively low background.

A complete study of this measurement has been performed for [1]. Here more details of that analysis and a few updates are provided.

2 Trigger strategy

The ATLAS triggers for B-physics allow the creation of both $J/\psi \to \mu\mu$ and $J/\psi \to ee$ data samples at LVL2. The $J/\psi \to \mu\mu$ trigger is based on the muon chambers and on information provided by the hadron calorimeters and the Inner Detector. The $J/\psi \to ee$ sample relies on the pion/electron separation provided by the TRT detector down to a minimum p_T of 0.5 GeV. The availability of two independent samples increases the total statistics to perform the sin2β measurement and gives the possibility of useful cross-checks.

The LVL1 trigger requirement for B-physics implies that both J/ψ samples will contain a muon with $p_T > 6$ GeV within the pseudorapidity range $|\eta| < 2.4$. The LVL2 trigger can be either an e^+e^- pair (with an electron p_T threshold of 0.5 GeV), an electron with $p_T > 5$ GeV or an additional muon with $p_T > 5$ GeV. Since it seems feasible to obtain a 3 GeV LVL2 muon trigger, in the following note we also consider this lower trigger threshold to estimate the event yields.

In the $J/\psi \to ee$ sample the additional lepton demanded by LVL1 trigger in the event has a crucial additional role. In fact, one of the methods used to tag the flavour at production of the B_d^0 which has decayed to $J/\psi K_s^0$ is to look for an additional lepton coming from the semileptonic

decay of the other ("opposite side") b-quark in the event (this technique is called "lepton tagging" and is discussed in more detail in Section 4.1). This implies that the $J/\psi \rightarrow ee$ sample is automatically tagged thanks to the LVL1 muon.

As the same technique can be used also in the $J/\psi \rightarrow \mu\mu$ sample, it is important to notice that in this case the two muons available after LVL2 can either be the two J/ψ legs or come one from the J/ψ and the other one from the opposite side b-quark. The third muon in these events (not in the triggers) is searched down to the lowest transverse momentum for muon identification in the detector (estimated to be 3 GeV). The lower p_T threshold on the lepton tagging muon is set to 5 GeV because of mistag rate considerations (see Section 4.1). If the LVL2 muon trigger threshold is set at 5 GeV, the LVL1 trigger muon can be either the tag muon or one of the two J/ψ legs. In the analysis only J/ψ with muons having minimum p_T of 5 and 3 GeV respectively are considered. This implies that if the LVL2 muon trigger threshold is set at 3 GeV, the case in which the LVL1 muon is the tag muon and both J/ψ legs have a minimum p_T of 3 GeV is excluded.

Electron triggering at LVL2, with a threshold set at 5 GeV, is also available thanks to the combined information from the TRT, the SCT and the EM calorimeter. In this case, the electron is used for lepton tagging and a second muon (not in the trigger) is searched in the event to make a J/ψ with the LVL1 trigger muon. It should be pointed out that, because of the LVL1 muon request, electron tagging cannot be applied to the $J/\psi \rightarrow ee$ sample.

Lepton tagging is not the only b flavour tagging method used in this analysis, so the presence of a third lepton in the event is not always required. Non-leptonic tagging methods (described in Sections 4.2 and 4.3) are not applied at trigger level. In case of $J/\psi \rightarrow \mu\mu$ events, the starting samples for the analysis are larger than in case of lepton tagging and have a J/ψ made with the 6 GeV muon trigger and a second muon of 3 or 5 GeV, depending on the LVL2 muon trigger threshold. While non-lepton tagging methods can also be applied to the $J/\psi \rightarrow ee$ sample and possibly combined with lepton tagging in order to increase the statistical tagging power, in this case there is no increase in the size of the sample as this is already set by the presence of the LVL1 muon.

3 Signal reconstruction

3.1 J/ψ reconstruction

The $B_d^0 \rightarrow J/\psi K_s^0$ samples were generated with PYTHIA in both J/ψ leptonic decay modes and fully simulated in the Inner Detector with GEANT. Offline cuts on the transverse momenta of the leptons from the J/ψ decay were the same as those imposed by the LVL1 and LVL2 thresholds. In the following, the notation $\mu 6\mu 3$ ($\mu 6\mu 5$) stands for events with one LVL1 muon and another muon with a p_T threshold of 3 GeV (5 GeV). Note that the $\mu 6\mu 5$ sample is a subset of the $\mu 6\mu 3$ one.

Track reconstruction in the entire Inner Detector was performed using the xKalman algorithm [2]. A special electron fit option was used in xKalman: for identified electrons (based on the TRT electron/pion separation), the reconstruction program includes, directly in the track-fitting procedure, a correction for possible energy losses due to bremsstrahlung.

Pairs of opposite-charge electrons (with $p_T > 0.5$ GeV) or muons ($\mu 6\mu 3$ or $\mu 6\mu 5$, as explained

above) were fitted to a common vertex and their invariant mass calculated. Only events where the two tracks could be successfully matched with the true Monte Carlo information (*Kine-match*) were considered. Successful fits (χ^2/d.o.f. < 6) were retained and, for the muon case, an invariant-mass cut with a window around the nominal J/ψ mass was applied (see Table 1). For the electron case, the window was set to be asymmetric in order to take into account the bremsstrahlung energy losses that create a long tail at small invariant masses. This energy loss depends on the amount of material traversed by the electrons and is larger in the end-cap than in the barrel region of the Inner Detector. Finally, a cut on the transverse decay length of the reconstructed J/ψ vertex, L_{xy}, was applied. The L_{xy} is defined as:

$$L_{xy} = \frac{\vec{R} \cdot \overrightarrow{p_T}}{\left\| \overrightarrow{p_T} \right\|}$$

where R is the distance between the primary and secondary vertices and p_T is the J/ψ reconstructed transverse momentum. All cuts (applied in cascade) for J/ψ reconstruction are detailed in Table 1.

Variable	**Cut**	**Efficiency**		
		J/ψ → e⁺e⁻	**J/ψ → μ6μ3**	**J/ψ → μ6μ5**
Acceptance	LVL1	96.7%	97.7%	98.5%
Kine-match + Pair fit quality	χ^2 / d.o.f. < 6	68.9%	93.4%	93.0%
p_T of reconstructed tracks	LVL2	99.9%	99.2%	98.8%
Mass window				
$J/\psi \rightarrow \mu^+\mu^-$	[-3σ,+3σ]		98.3%	98.1%
in barrel ($\lvert\eta\rvert$ < 0.7)	σ = 30 MeV			
in end-caps ($\lvert\eta\rvert$ > 0.7)	σ = 40 MeV			
$J/\psi \rightarrow e^+e^-$ in barrel ($\lvert\eta\rvert$ < 0.7)	[-5σ,+3σ]	86.2%		
	σ = 53 MeV			
in end-caps ($\lvert\eta\rvert$ > 0.7)	[-7σ,+3σ]			
	σ = 63 MeV			
J/ψ decay length	L_{xy} > 250 μm	77.4%	86.9%	88.9%
Overall		44.4%	77.3%	78.9%

Table 1 Cuts applied for the J/ψ reconstruction and relative efficiencies. Cuts are applied in cascade. The LVL1 acceptance includes only the muon p_T and η cuts explained in the text.

For events passing the LVL1 trigger requirement (muon with p_T > 6 GeV in $|\eta|$ < 2.4), the J/ψ reconstruction efficiency is about 44 % in the electron channel and about 77 % in the muon channel (LVL2 trigger muon threshold at 3 GeV). These figures do not include the lepton trigger and identification efficiencies (see Section 3.3). The lower reconstruction efficiency in the electron channel is due to bremsstrahlung energy-loss effects causing the electrons to be lost in the reconstruction and causing the J/ψ to fail some of the cuts. The lower efficiency of the L_{xy} cut on the $J/\psi \rightarrow ee$ sample with respect to the $J/\psi \rightarrow \mu\mu$ sample is due to the use of a fixed cut (250 μm) for both samples even if the two samples have a different p_T spectrum: the average p_T of the signal B is 17 GeV in the $J/\psi \rightarrow ee$ sample and 25 GeV in the $J/\psi \rightarrow \mu\mu$ sample (see also

Section 3.3, where the selection cuts on the reconstructed B_d^0 vertex are discussed). Further studies seem to be required, both in the track reconstruction phase and in the selection of offline cuts, to improve the efficiency for reconstructing J/ψ.

The invariant-mass distributions for the electron and muon cases are shown in Figures 1 and 2, respectively. The distributions include only events in which the two reconstructed leptons have been successfully matched with the true Monte Carlo leptons from the J/ψ decay. The resolutions were estimated to be about 40 MeV (muons) and 60 MeV (electrons), where the resolution for the electron case was estimated by fitting only the symmetric core of the distribution.

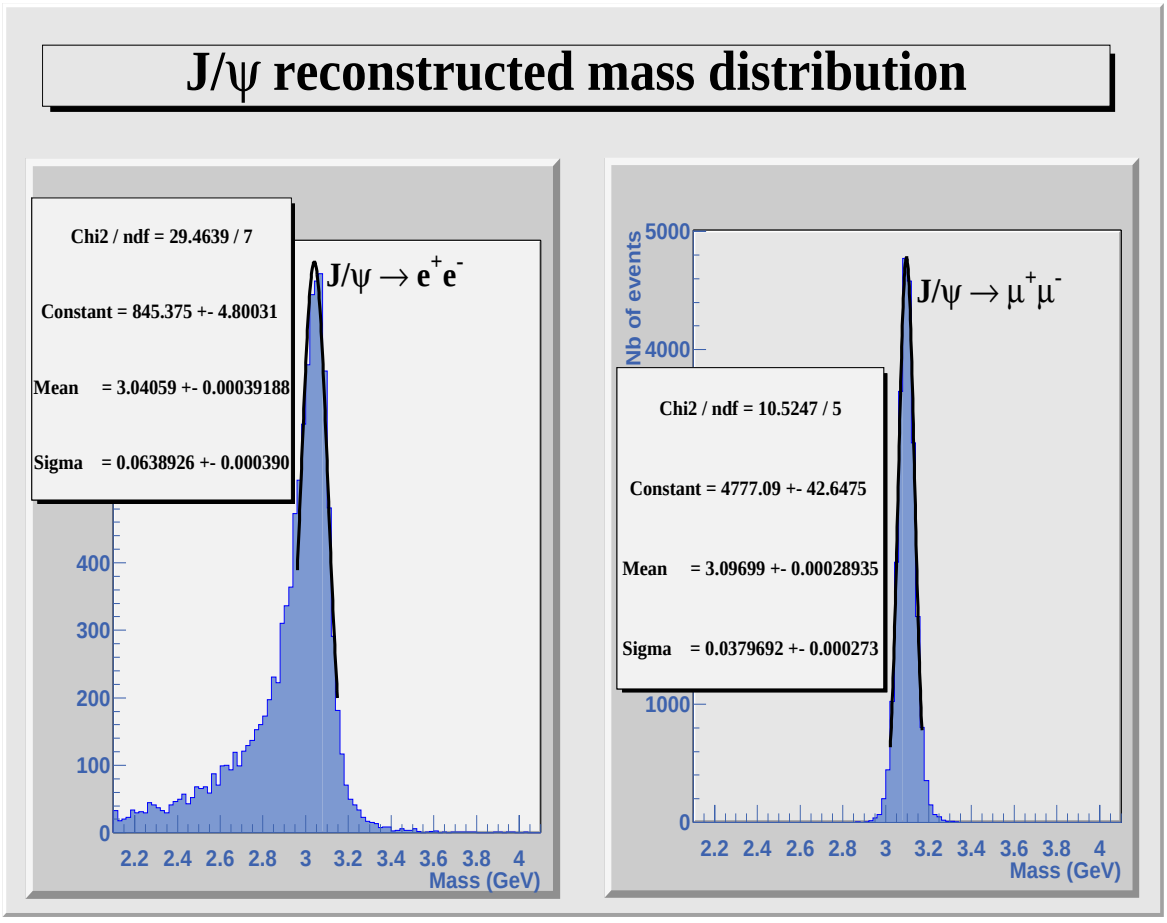

Figure 1 Invariant-mass distribution of $J/\psi \to e^+e^-$ (signal only).

Figure 2 Invariant-mass distribution of $J/\psi \to \mu^+\mu^-$ (signal only) for events with the LVL2 trigger muon p_T threshold at 3 GeV.

3.2 K_S^0 reconstruction

The reconstruction of the decay $K_S^0 \to \pi^+\pi^-$ is described in detail in [3]. K_S^0 vertices are searched for by looping on all opposite-charge track pairs (tracks previously identified as leptons are excluded) with a minimum p_T threshold of 0.5 GeV. The decay vertex was reconstructed using three-dimensional vertexing, and the track pair was chosen as a K_S^0 candidate if a vertex was found in a fiducial cylinder defined by the minimum number of precision hits required by the pattern recognition program to reconstruct a track. In this analysis we accept K_S^0 which have a decay radius between 1 cm and 37 cm and within $|z| < 210$ cm (corresponding to a request of 6

precision hits in the reconstruction), and if the invariant mass of the pair was compatible with the K_s^0 mass. The lower cut on the decay radius rejects the combinatorial background. Cuts are listed in Table 2.

Variable	Cut	Efficiency
Pair fit quality	χ^2 / d.o.f. < 50	47.9%
Mass window	[-3σ,+3σ] σ = 6.6 MeV	91.0%
Vertex detachment	L_{xy} > 1cm	93.9%
Overall		40.9%

Table 2 Cuts applied for the K_s selection after J/ψ reconstruction.

For events in which a J/ψ has been successfully reconstructed, the total K_s^0 reconstruction efficiency is about 41%. This figure includes the acceptance for a K_s^0 decay inside the fiducial volume delimited by the R and z cuts listed above, the tracking efficiency and the efficiency of the selection cuts (cuts on fit probability, mass window and transverse decay length from the primary vertex). The K_s^0 mass resolution is about 4.5 MeV for K_s^0 decays at low radii and increases to up to 7 MeV towards the external border of the fiducial decay volume.

3.3 B_d^0 reconstruction

Leptons and pions coming from J/ψ and K_s^0 candidates which survived the selection described above were used in reconstructing $B_d^0 \to J/\psi K_s^0$ decays. The B_d^0 was obtained by performing a three-dimensional kinematic fit to the four tracks and applying vertex and mass constraints on both the $\mu^+\mu^-$ and $\pi^+\pi^-$ systems. At the same time, the momentum of the K_s^0 (B_d^0) was required to point to the J/ψ (primary) vertex. Cuts on the B_d^0 candidate proper decay time and on its transverse momentum were also applied. The proper decay time is defined as:

$$\tau = \frac{L_{xy} \cdot M_B}{\left\| \overrightarrow{p_T} \right\|}$$

where L_{xy} is the radial vertex separation in the transverse plane (defined in Section 3.1), M_B is the B_d^0 mass and $\left\| \overrightarrow{p_T} \right\|$ is the reconstructed B_d^0 transverse momentum. The efficiencies of the cuts are listed in Table 3. The figures do not include lepton identification efficiencies. The higher efficiency of the proper decay time cut in the $J/\psi \to ee$ sample with respect to the $J/\psi \to \mu\mu$ samples is due to a previous cut on the J/ψ L_{xy} decay length (see Section 3.1): the L_{xy} cut (identical on both samples) is softer on the muon samples (which have a higher p_T spectrum) so making the proper decay time cut apparently harder (and *vice versa* on the electron sample). The correlation between these two cuts will be further investigated.

A mass resolution of 24 (18) MeV (as shown in Figures 3 and 4) and a transverse decay-length resolution of 68 (64) μm were estimated for the reconstructed B_d^0 meson in events in which the J/ψ decayed to electrons (muons).

After the first three years of running at low luminosity, corresponding to an integrated luminosity of 30 fb^{-1}, it is estimated that ATLAS will reconstruct 14,400 $J/\psi K_s^0$ decays in the $J/\psi \to e^+e^-$

Variable	Cut	Efficiency		
		$J/\psi \to e^+e^-$	$J/\psi \to \mu 6 \mu 3$	$J/\psi \to \mu 6 \mu 5$
Successful kinematic fit	loose χ^2	96.3%	95.8%	95.9%
Mass window	$[-3\sigma,+3\sigma]$			
$J/\psi \to \mu^+\mu^-$		90.2%		
in barrel ($\|\eta\| < 0.7$)	σ = 16 MeV			
in end-caps ($\|\eta\| > 0.7$)	σ = 21 MeV			
$J/\psi \to e^+e^-$			93.5%	92.6%
in barrel ($\|\eta\| < 0.7$)	σ = 21 MeV			
in end-caps ($\|\eta\| > 0.7$)	σ = 30 MeV			
Proper decay time	$\tau > 0.5$ ps	91.0%	84.1%	83.2%
Fit quality	χ^2 / d.o.f. < 6	86.3%	95.5%	95.6%
Transverse momentum	$p_T > 5$ GeV	96.3%	100%	100%
Overall		65.7%	71.9%	70.6%

Table 3 Cuts applied for B_d^0 selection after K_S^0 reconstruction. Cuts are applied in cascade. The overall efficiency (last row) refers to events with a reconstructed J/ψ and K_S^0

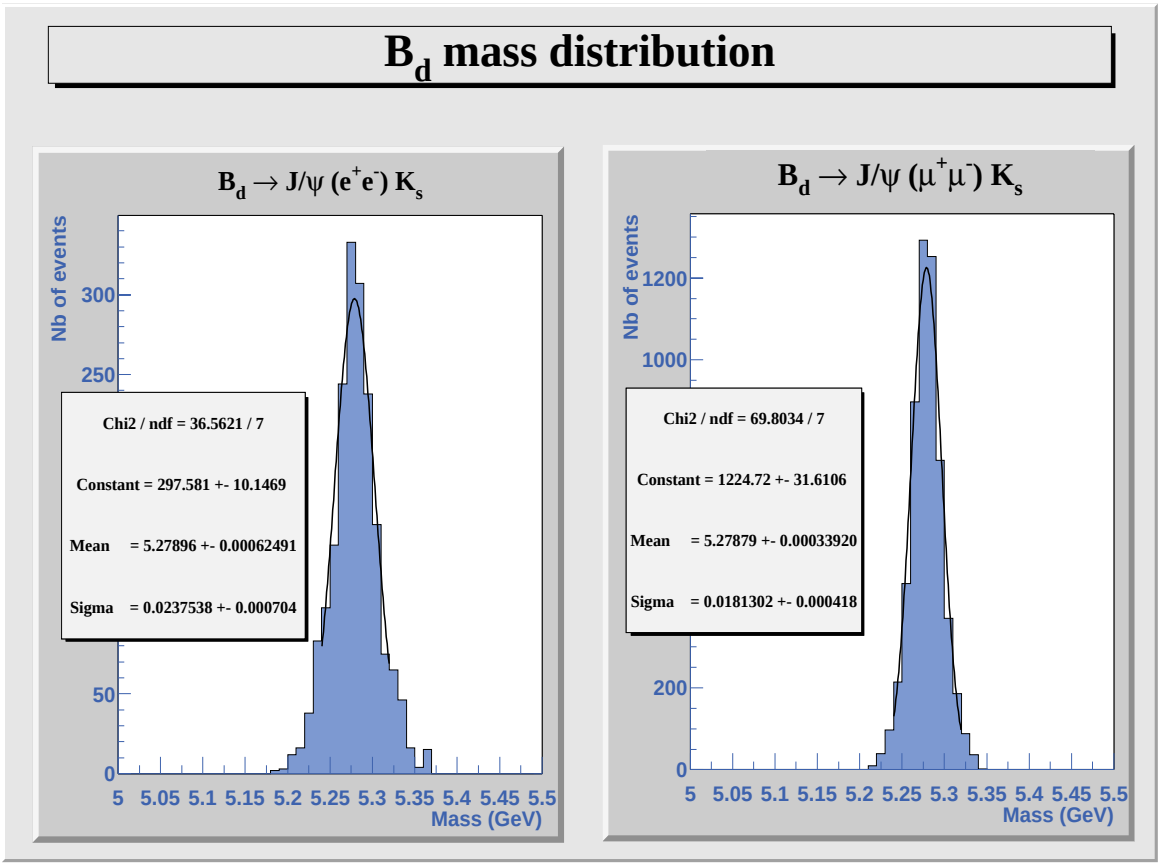

Figure 3 Invariant-mass distribution of B_d^0 meson in $J/\psi \to e^+e^-$ events (signal only).

Figure 4 Invariant-mass distribution of B_d^0 meson in $J/\psi \to \mu^+\mu^-$ events (signal only) with the a LVL2 trigger muon p_T threshold at 3 GeV.

channel and 473,550 (219,690) events in the $\mu^+\mu^-$ channel, assuming a LVL2 trigger threshold of 3 GeV (5 GeV) for the second muon. The relatively low number of $J/\psi \to e^+e^-$ events is due to the requirement of an additional muon which provides the LVL1 trigger and can be used for tagging the flavour of the B_d^0 at production. Besides all the selection cuts described above, these numbers also include the trigger efficiencies and the estimated efficiencies of the detector to identify electrons and muons listed below in Table 4. The LVL2 trigger efficiency is assumed to be 100% for events which are selected after reconstruction.

Particle type	Efficiency (%)
LVL1 trigger muon	85
other muons with $p_T > 3$ GeV	90
other muons with $p_T > 5$ GeV	95
electrons	75

Table 4 Trigger and lepton identification efficiencies used in the calculation of the event yields.

4 Flavour tagging

To perform a measurement of the CP-violating asymmetry, it is necessary to know the flavour of the neutral B meson at production. Various methods have been developed for this purpose along the years, mainly by the LEP experiments and by CDF. Flavour tagging can be divided in two categories: Opposite-Side Tagging (OST) and Same-Side Tagging (SST). In the former case the algorithm deduces the flavour by looking at the decay products of the other *b*-quark in the event (the opposite side). In the latter case the algotithm looks at the particles accompanying the B-meson under study (the same side). In this section, a brief description of the tagging algorithms developed so far for this analysis is given and the performance summarized. Each algorithm has been optimized by adjusting its parameters to maximise the quality factor $Q = \varepsilon D_{tag}^2$ that determines the statistical precision on the asymmetry measurement. Here, D_{tag} (dilution factor) and ε (tagging efficiency) are defined as follow. The dilution D_{tag} measures the number of times we have a right sign tag:

$$D_{tag} = \frac{N^+ - N^-}{N^+ + N^-}$$

where N^+ is the number of right sign tags and N^- is the number of wrong sign tags. The efficiency ε is defined as the number of tagged events over the total number of reconstructed B mesons:

$$\varepsilon = \frac{N_{tag}}{N(B)}$$

where $N_{tag} = N^+ + N^-$.

4.1 Lepton tagging

In the lepton-tagging technique, an additional lepton is searched for in the event, with the assumption that this tag lepton originates from a semileptonic decay of the other *b* quark in the

event. This method is known to have low efficiency (due to the low *b* semileptonic branching ratio of about 10% and to the kinematic cuts), but good purity. However, in the $J/\psi \to e^+e^-$ sample this method is fully efficient due to the presence of the trigger muon. In the $J/\psi \to \mu^+\mu^-$ sample, an additional lepton (muon or electron) with $p_T > 5$ GeV is searched for. In case the tag lepton was a muon (so that there are three muons in the event), the LVL1 trigger muon could be either one of the J/ψ legs or the tag muon. The total lepton-tagging efficiency in the $J/\psi \to \mu^+\mu^-$ sample is about 0.04 (electron or muon tag).

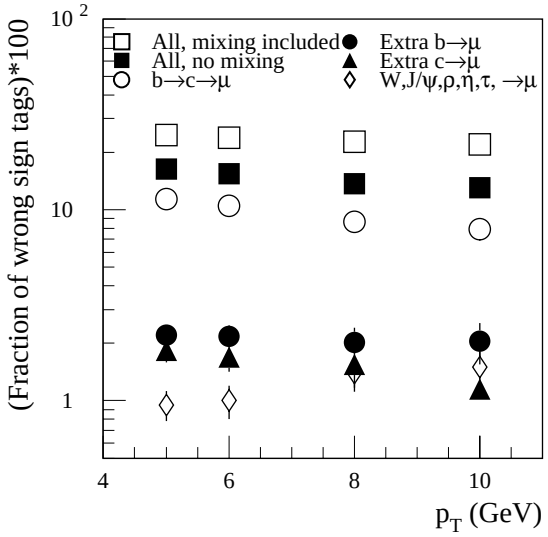

Figure 5 Muon wrong-tag fraction as a function of the tag p_T threshold. This plot is made for the case where the decay $J/\psi \to \mu^+\mu^-$ gives rise to a muon with $p_T > 6$ GeV. At tag $p_T > 6$ GeV, the average p_T of the signal-B is 26 GeV.

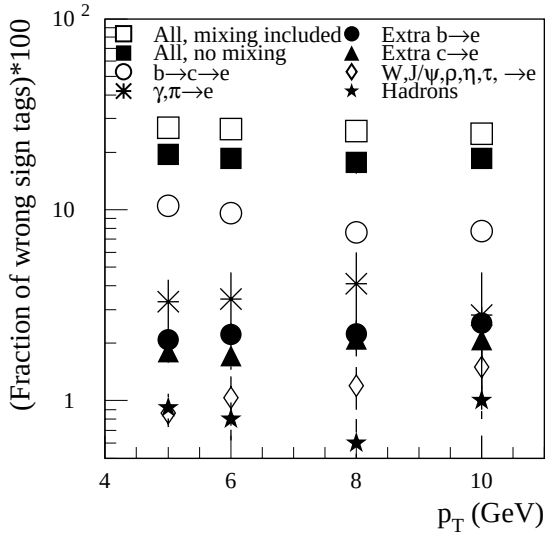

Figure 6 Electron wrong-tag fraction as a function of the tag p_T threshold. This plot is made for the case where the decay $J/\psi \to \mu^+\mu^-$ gives rise to a muon with $p_T > 6$ GeV. At tag $p_T > 5$ GeV, the average p_T of the signal-B is 25 GeV.

The mistag rate with lepton tagging was extensively studied in a large inclusive-muon sample and double-checked, with smaller statistics, in samples of $B_d^0 \to J/\psi K_s^0$ decays. The dependence of the mistag rate on the tag lepton transverse momentum threshold is shown in Figures 5 and 6 for muons and electrons respectively. It can be seen that the wrong-tag fraction decreases with increasing tag p_T threshold and is dominated by $b \to c \to l$ cascade decays. The mistag rate depends on the p_T of the signal B-hadron as well as on the p_T of the tag lepton. With increasing p_T of the signal B-hadron, the wrong-tag fraction increases for a fixed tag p_T threshold. This is due to the fact that, with increasing p_T of the signal B-hadron, the p_T of the other B tends to increase, resulting in an increasing probability for the leptons from cascade decays to pass the p_T threshold for the tag. This can be seen in Figure 7, which shows the wrong-tag fraction as a function of the signal

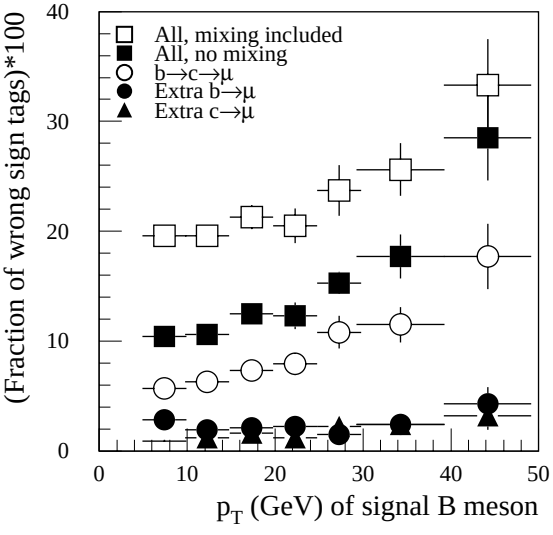

Figure 7 Muon wrong-tag fraction as a function of the signal B-hadron p_T. The tag muon was required to have $p_T > 6$ GeV.

B-hadron p_T, when the tag p_T was fixed to 6 GeV.

For muon tagging of the $J/\psi \to \mu^+\mu^-$ sample, a mistag rate $\omega_{tag} = 0.24$ was applied in the analysis. Here the average p_T of the B_d^0 is about 25 GeV. For muon tagging of the $J/\psi \to e^+e^-$ sample, the wrong-tag fraction was lower, $\omega_{tag} = 0.21$, due to the lower p_T of the signal-B (17 GeV on average). Contributions to the mistag rate from hadrons misidentified as muons and from decays in flight of pions and kaons were found to be negligible. Efficiencies and mistag rates are summarized in Table 6.

For electron tagging of the $J/\psi \to \mu^+\mu^-$ sample, the fraction of wrong tags was 0.27 with a 5 GeV threshold. The contributions to the mistag rate from misidentified hadrons (about 1%) and from conversions (about 2%) were estimated using fully simulated Monte Carlo samples. The hadron rejection factor was about 1800, corresponding to a 75% electron efficiency — the electron was identified by using both the e.m. calorimeter and the TRT (see [4]). The conversion-removal algorithm, which is similar to the one described in [4] for the $H \to \gamma\gamma$ analysis has not yet been fully optimized for this analysis. Efficiencies and mistag rates are summarized in Table 6.

4.2 B-π correlation tagging

The B-π correlation tagging is an SST technique as it uses charged pions associated with the B_d^0 that has decayed to $J/\psi K_S^0$ to determine the flavour of the B meson. The method presented here is similar to the one discussed in [5]. During the process of a $\bar{b}$-quark fragmentation to B_d^0, pions which are charge-correlated to the B meson flavour can be produced by mainly two different mechanisms [6] (see Figure 8):

- The $\bar{b}$ quark picks up a d quark from the quark-sea to form a B_d^0, so making available a $\bar{d}$ quark to form a π^+.

- A B^{**} excited state is produced which then decays to a B_d^0: $B^{**} \to B^{(*)0}\,\pi^+$.

The symbol B^{**} is a common shorthand for orbitally excited states of B mesons. These states have exactly the same quark content as the B, but orbital angular momentum equal to 1 (the total momentum J=L+S is indicated by a subscript).

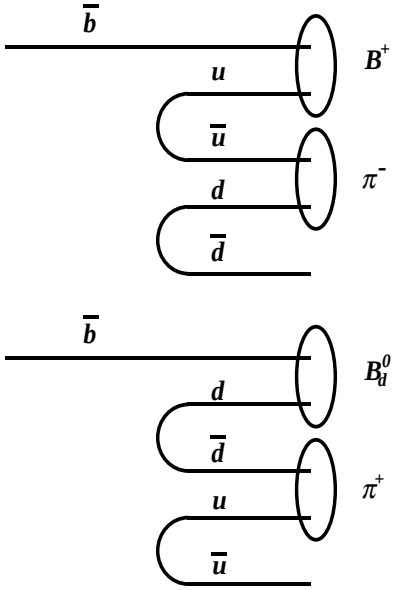

Figure 8 Possible mechanisms for pion production during the fragmentation of charged (upper figure) and neutral (lower figure) B mesons (from [5]).

The B^{**} mesons' decays of interest for us are the ones giving a B^0 (or B^{*0}) and a charged pion. If a B^{*0} is present it decays to $B^0\gamma$. The main properties of these resonances are listed in Table 5 [7][8]. We do not include B^{**} which decay to neutral pions or to photons.

For both charge-correlated pion production mechanisms, we notice that a π^+ is associated to B_d^0 while a π^- suggests the production of a $\overline{B_d^0}$. In the following, no attempt will be made to separate the two contributions. The associated particle will be called "pion" in the following al-

though no attempt will be made to identify it as such.

The algorithm selects charged-particle tracks contained in a cone $\Delta R < 0.7$ around the reconstructed B meson direction, with $|d_0|/\sigma_{d_0} < 3$ (where d_0 is the transverse impact parameter of the pion) and with 0.5 GeV < p_T < 4.0 GeV. If more than one particle survives this selection, the one with the highest momentum component along the reconstructed B direction, p_L^{rel}, is selected (see Figure 9 for the definition of the variables used in the selection). This set of cuts provides the highest quality factor, although other choices provided similar results within the statistical uncertainty. The results for the efficiency and the dilution factor for this algorithm are presented in Table 6.

Label	S	J^P	Mass (GeV)	Width (GeV)	Decays to
B_0^{*+}	1	0^+	5.630	0.100	$B^0\pi^+$
B_1^+	0	1^+	5.742	0.021	$B^{*0}\pi^+$
B_1^{*+}	1	1^+	5.642	0.100	$B^{*0}\pi^+$
B_2^{*+}	1	2^+	5.754	0.025	$B^{*0}\pi^+$,$B^0\pi^+$

Table 5 Properties of the B** resonances considered in the text.

4.3 Jet charge tagging

Another possibility to tag the flavour of the B meson consists in studying the total charge of the tracks produced nearby the B meson. This charge is correlated to the flavour of the B meson as in the B^{**} tagging ($\bar{b}$ quark implies positive charge, b quark a negative one). An algorithm is required in order to select only tracks likely to belong to the B fragmentation. The charge is then defined as an average of the tracks charge in the cluster, weighted with a function of their momenta:

$$Q_{jet} = \frac{\sum_{i=1}^{n} q_i \cdot w_i}{\sum_{i=1}^{n} w_i}$$

where q_i is the track charge and w_i is a function of the track momentum.

Although jet-charge tagging (JC) can be applied to both the B_d^0 jet and to the opposite jet, for the time being it was applied only to the same-side jet.

The algorithm included in the charge calculation all tracks with $p_T > 0.5$ GeV, $|d_0| < 1$ cm and $|\Delta z| < 5$ cm (where Δz is the difference between the z_0 of the track and the z-coordinate of the primary vertex), contained inside a cone $\Delta R < 0.8$ around the B direction[1] (see Figure 9). The four particles identified as the B_d^0 decay products were excluded. Then the jet charge Q_{jet} was calculated and the right (wrong) sign events were defined as those having $Q_{jet} > +c$ ($Q_{jet} < -c$), where c is a tunable cut. The value of the cut c and the weights w_i were optimized to maximise the quality factor $Q = \varepsilon D_{tag}^2$. In the end $w_i = p_{Ti}^k$, where k = 1.25 (1.0) for the $J/\psi \to e^+e^-$ ($J/\psi \to \mu^+\mu^-$) sample, and c = 0.26 for both J/ψ decay channels were chosen. Different sets of cuts provided similar results within the statistical uncertainties. The results are summarized in Table 6.

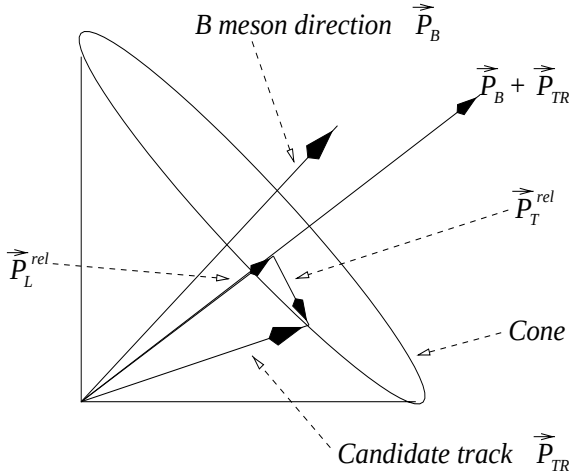

Figure 9 Definition of the variables used (from [5]) in the tagging algorithm.

	$B_d^0 \to J/\psi(ee)K_S^0$			$B_d^0 \to J/\psi(\mu 6 \mu 3)K_S^0$			$B_d^0 \to J/\psi(\mu 6 \mu 5)K_S^0$		
tag	ε_{tag}	D_{tag}	**Q**	ε_{tag}	D_{tag}	**Q**	ε_{tag}	D_{tag}	**Q**
OST: e	n / a	n / a	n / a	0.012	0.46	0.0025	0.016	0.46	0.0034
OST: μ	1	0.57	0.32	0.025	0.52	0.0068	0.025	0.52	0.0068
SST: B-π	0.80	0.14	0.016	0.82	0.16	0.021	0.84	0.17	0.024
SST: JC	0.71	0.12	0.010	0.64	0.17	0.018	0.66	0.18	0.021

Table 6 Efficiencies, dilutions and quality factors for the tagging algorithms considered in the analysis (n/a = not available).

5 Signal event yields

The total number of events after tagging is summarized in Table 7 for each sample for an integrated luminosity of 30 fb^{-1}.

Since the lepton tag purity is much higher than the B-π tag purity, the lepton tag was used whenever it was available. The B-π tag was used only if there was no lepton tag. The highest statistical tagging power would be achieved by combining all available tagging information on an event-by-event basis. A study of the tag combination has not yet been performed. Jet-charge tags have proven, as expected, to be highly correlated with B-π tags, and since the B-π tag purity

1. $\Delta R = \sqrt{\Delta\varphi^2 + \Delta\eta^2}$ (where φ and η are the azimuthal angle and the pseudorapidity, respectively) is the distance between the track and the B direction in the η–φ space.

	$B_d^0 \to J/\psi(ee)K_S^0$		$B_d^0 \to J/\psi(\mu 6 \mu 3)K_S^0$		$B_d^0 \to J/\psi(\mu 6 \mu 5)K_S^0$	
	Signal	**Background**	**Signal**	**Background**	**Signal**	**Background**
Untagged	14,400	900	480,000	15,300	220,000	5,000
Lepton tags	14,400	900	17,700	1,600	8,800	500
e tag	n / a	n / a	5,800	500	3,500	200
μ tag	14,400	900	11,900	1,100	5,300	300
B-π tags	11,600	900	390,700	15,300	184,100	5,000
B-π tags with no lepton tag	n / a	n / a	376,100	13,700	176,700	4,500
Jet Charge	10,200	900	307,200	14,500	136,400	4,800

Table 7 Expected number of tagged events and relative background for each sample for an integrated luminosity of 30 fb^{-1}. The e- and μ- tag samples are subclasses of the lepton-tagged sample.

was higher than the jet-charge-tag purity, only B-π tags were used.

6 Background estimate

The background to the $B_d^0 \to J/\psi K_S^0$ decay was studied using large samples of J/ψX and μ6X events. The first sample is an inclusive sample of J/ψ from B's which was produced with the same lepton-p_T thresholds as for the signal sample. This sample was used to give an estimate of the background coming from B decays containing a true J/ψ in the final state. Background contributions can come from the combination of a true J/ψ with K_S^0 candidates from various sources: true K_S^0 from B-hadron decays, true K_S^0 from the fragmentation, and fake K_S^0.

The μ6X sample contained events with muons from semileptonic B-hadron decays with a minimum muon transverse momentum of 6 GeV. This sample was used to estimate the background from fake J/ψ's (arising from lepton–lepton, lepton–hadron and hadron–hadron pairs) reconstructed in association with a true or a fake K_S^0. The background from prompt J/ψ's has not yet been studied for this channel. The background samples were processed using the fast simulation program briefly described in the next paragraph. However, good agreement was found with results obtained from smaller-statistics samples of fully-simulated background events.

6.1 Fast simulation

The large number of background events needed to be processed in order to perform a reliable estimate of the background to the decay $B_d^0 \to J/\psi K_s^0$ puts serious requests on the CPU time needed. In order to speed up the process, the background samples were simulated with a fast simulation program. The fast simulation program replaces the full GEANT simulation with a parametrized one. The parametrization is applied to the 4-momenta of the generated particles and is a function of p_T and η (and also of the decay radius in case of pions, in order to be able to describe also pions coming from the decay of K_s^0). The parametrization is established studying in detail the resolutions (including tails) of the five helix parameters of the tracks in fully-simulated samples and outputs the smeared five helix parameters of the track and the corresponding covariance matrix. The parametrization, described in detail in [9], handles differently muons, electrons and pions.

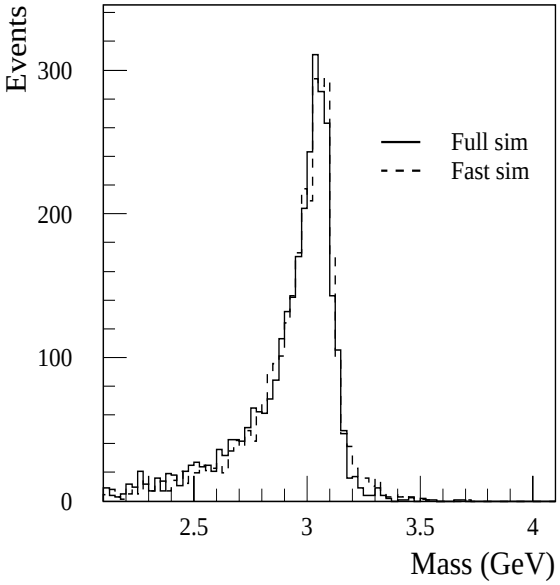

Figure 10 Comparison between full (solid line) and fast (dashed line) simulation for $J/\psi \to e^+e^-$.

Muon resolutions in fully simulated samples did not show appreciable tails and so they were parametrized with Gaussian functions as a function of p_T and η.

Electron resolutions, on the contrary, showed a non-Gaussian behaviour which is due to the interactions with the material of the Inner Detector. To take this effect into account, electron distributions were parametrized also as a function of a single hard bremsstrahlung, chosen at random from the appropriate distribution. The agreement between full and fast simulation is good as can be seen from Figure 10 which shows the invariant mass of a $J/\psi \to ee$ decay, obtained using the two simulation programs.

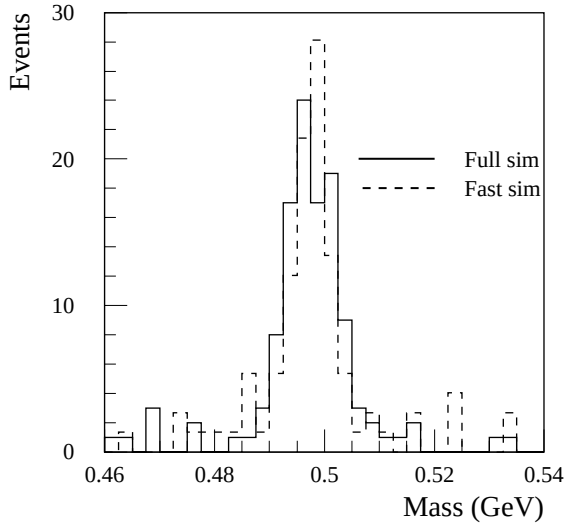

Figure 11 Comparison between full (solid line) and fast (dashed line) simulation for $K_s^0 \to \pi^+\pi^-$.

The parametrization for pions was established studying the resolutions of the five track parameters in fully-simulated samples. The total sample was divided into bins of p_T, η and decay radius R in order to be able to describe also the pions from K_s^0. In each bin, the track parameter resolutions were described as the sum of two Gaussians in order to take into account also the presence of tails. While an exponential description of the tails might have been more appropriate in some cases, the two-Gaussian description provides good results and allows to take into account correlations in a more straightforward way. As discussed in [9], this method allows to obtain a parametrization of the full covariance matrix (including the correlation terms) as a

function of p_T, η and R. This parametrization was used to smear the five generated pion-track parameters in the fast-simulation program. The K_s^0 mass distribution obtained using this method is compared to the one obtained with full simulation in Figure 11; reasonable agreement is observed between the two.

6.2 Background yields

After having applied the fast simulation program to the background samples, the samples are processed using the same analysis program and offline cuts used for the fully simulated signal samples. The total number of surviving background events is presented in Table 7. These numbers use the same lepton efficiency as for the signal events (see Table 4) plus the efficiency for pions and K_s^0 reconstruction listed in Table 8 (these additional correction factors are needed as the fast simulation does not simulate the pion reconstruction efficiency).

Particle type	Efficiency (%)
Pions	90
K_s^0	84.9

Table 8 Particle identification efficiencies used in the calculation of the background yields.

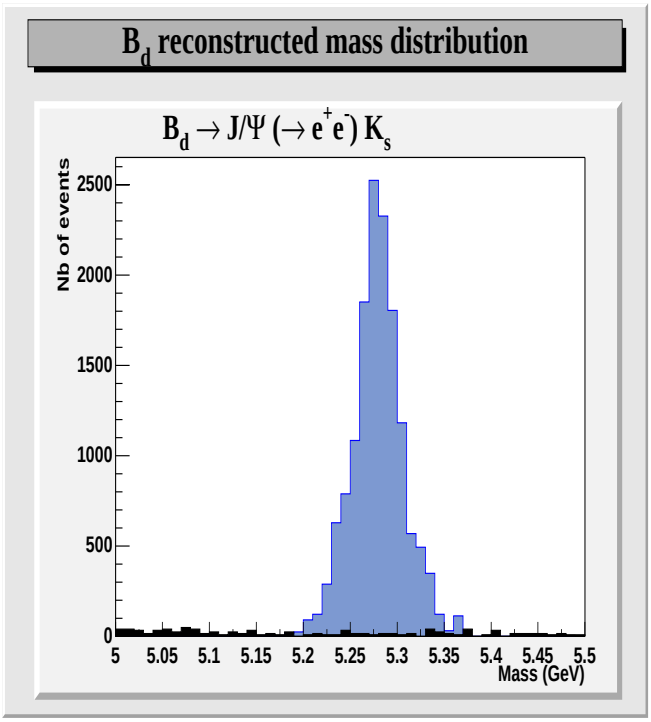

Figure 12 Invariant-mass distribution of the B_d^0 peak in the muon-tagged $J/\psi \to e^+e^-$ channel (grey histogram) with superimposed the estimated background contribution (black histogram).

B-π tagging has not been studied on the background samples. Conservatively, a pessimistic 95% B-π tagging efficiency has been assumed for the background events. In all the samples, the biggest background contribution comes from true J/ψ background events. The background level under the $B_d^0 \to J/\psi K_s^0$ peak is rather small including all samples (see Figure 12).

7 The statistical accuracy of the sin2β measurement

The accuracy of the sin2β measurement was estimated with a fit to the time-dependent asymmetry distribution with a function of the form $A = D\sin 2\beta \sin(\Delta m_d t)$, where D is the overall dilution factor. The time-dependent asymmetry was modelled including dilution factors from background and from tagging. An input value of $\sin 2\beta = 0.6$ was assumed for this study. The only free parameter of the fit was sin2β. The proper time of the B-decay was histogrammed using bins of width of 0.83 ps (corresponding to about 250 μm in decay length). Due to the cut on the decay proper time used in the selection, the measurement was made for $\tau(B) > 0.5$ ps. The proper time

resolution, estimated using the fully simulated signal sample, is 0.073 ps.

The results of the fit using lepton tagging and B–π tagging in the various samples considered are presented in Table 9. In the table, lepton tagged events have been removed from the B-π tagged samples, leaving statistically independent samples. Since in the J/ψ(e^+e^-) class all the events have a muon tag, no events are left in the B-π tagged sample. Note that the statistical precision from a number of different samples and tagging methods is comparable, allowing meaningful cross-checks to be made between them.

	J/ψ(e^+e^-)	J/ψ(μ6μ3)	J/ψ(μ6μ5)
Lepton tagging	0.018	0.023	0.030
B–π tagging	n / a	0.015	0.019

Table 9 Estimate of the error on sin2β using a time dependent analysis in each of the samples considered for lepton tagging and B–π tagging after three years of running at low luminosity.

As the $B_d^0 \to J/\psi(ee)K_s^0$ sample is statistically independent from the $B_d^0 \to J/\psi(\mu\mu)K_s^0$ ones, results from the two samples can be combined in a straightforward way. Using lepton tagging combined with B-π tagging, the estimated uncertainty on sin2β, with 30 fb^{-1} of data, is given in Table 10.

	J/ψ(ee) + J/ψ(μ6μ3)	J/ψ(ee) + J/ψ(μ6μ5)
B-π + lepton tagging	0.010	0.012

Table 10 Estimated statistical error on sin2β combining B-π tagging and lepton tagging (30 fb^{-1}).

8 Systematic uncertainties

Although systematic uncertainties in the sin2β measurement can in principle originate from many sources, previous studies have shown the overall systematic error to be small [10]. Contributions to the systematic uncertainty come from the production asymmetry of B_d^0 and $\overline{B_d^0}$ mesons, from asymmetries in the tagging efficiency and in the background, and from uncertainties in the determination of the various dilution factors. All these uncertainties need to be controlled in order not to spoil the statistical precision.

Many of the potential sources of systematic uncertainty can be controlled using the channels $B^+ \to J/\psi(\mu\mu)K^+$ and $B_d^0 \to J/\psi(\mu\mu)K^{*0}$ (where $K^{*0} \to K^+\pi^-$). For the first channel the results for charged B-mesons need to be extrapolated to the neutral case which may introduce some model dependence. For the second channel, the results are obtained directly for B_d^0 particles, making allowance for the flavour oscillations. The reconstruction of these so-called control channels is discussed below before estimates of the systematic uncertainties are presented.

The availability of many tagging algorithms and the large statistics of tagged and untagged signal and control samples provide the flexibility to perform internal cross-checks of the analysis. The $B^+ \to J/\psi(\mu\mu)K^+$ and $B_d^0 \to J/\psi(\mu\mu)K^{*0}$ samples can be used to measure the wrong-tag fraction for the various tagging methods and also the charge asymmetry in the tagging efficiencies. For all these studies, it is important to be able to reconstruct large statistics of control samples, so that the systematic errors will not appreciably degrade the statistical error on sin2β.

8.1 Control channels

8.1.1 Reconstruction of $B^+ \to J/\psi(\mu\mu)K^+$

This decay (as well as the $B_d^0 \to J/\psi(\mu\mu)K^{*0}$ decay described in Section 8.1.2) was studied using a sample of events generated with PYTHIA and fully simulated inside the Inner Detector. Only J/ψ decays to muon pairs were considered.

The trigger selection for this channel was the same as for the $B_d^0 \to J/\psi(\mu\mu)K_S^0$ decay channel. However, in the reconstruction the J/ψ vertex is always made of one muon with $p_T > 6$ GeV (LVL1 trigger muon) and one muon with $p_T > 3$ GeV (5 GeV) depending on the LVL2 trigger. The other selection cuts on the J/ψ are similar to those described in Section 3.1. Once a J/ψ was successfully reconstructed, the event was searched for a track (the 'kaon') satisfying the criteria given in Table 11. The track was required to be inconsistent with coming from the primary vertex at the one standard deviation level ($|d|/\sigma_d > 1$, where d is the track impact parameter and σ_d is its error). The two muons and the kaon were then fitted to a common vertex applying a mass constraint to the J/ψ and requiring the total momentum at the B vertex to point to the event primary vertex. Cuts applied to the B vertex are summarized in Table 12, together with their relative efficiencies.

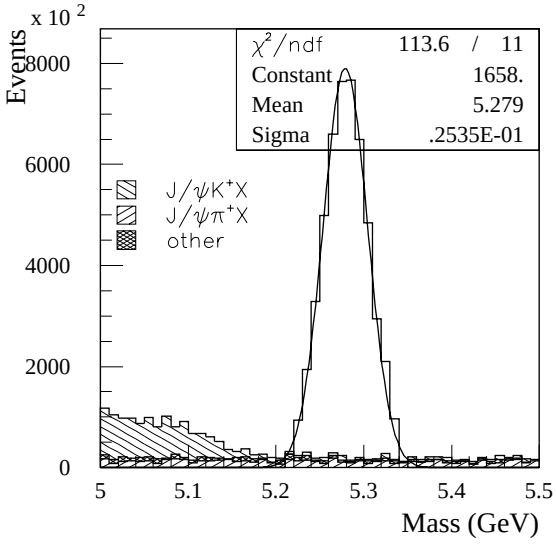

Figure 13 Invariant-mass distribution for the decay $B^+ \to J/\psi(\mu 6 \mu 3)K^+$ (open histogram) with superimposed the estimated background contribution (shaded histograms).

Variable	Cut	Efficiency
Transverse momentum	$p_T > 1.5$ GeV	75.3%
Separation from primary vertex	$\|d\|/\sigma_d > 1$	92.9%
Overall		69.9%

Table 11 Cuts applied for the K^+ selection after J/ψ reconstruction.

The mass peak is shown in Figure 13; the mass resolution is about 25 MeV. The number of signal events expected for an integrated luminosity of 30 fb^{-1} is shown in Table 13 for both LVL2 trigger options. Trigger and lepton efficiencies listed in Table 4 are used to rescale the total number of events. Also shown in this table are the numbers of untagged background events estimated using the inclusive $J/\psi X$ sample, fast-simulated as described in Section 6.1. Efficiencies listed in Table 8 are applied. The backgrounds from fake J/ψ and prompt J/ψ have not yet been included in this study. However, in the background estimate for the signal $B_d^0 \to J/\psi(\mu\mu)K_s^0$, the dominant background was found to originate from real J/ψ from B-decays. The selection cuts for this channel may need further optimization to improve the signal-to-background ratio.

The background shape (see Figure 13) is made of three components. The first one (31% of the to-

Variable	Cut	Efficiency
Successful kinematic fit	loose χ^2	99.3%
Mass window in barrel ($\|\eta\| < 0.7$) in end-caps ($\|\eta\| > 0.7$)	$[-3\sigma,+3\sigma]$ σ = 16 MeV σ = 21 MeV	92.2%
Fit quality	χ^2 / d.o.f. < 6	99.6%
Transverse momentum	$p_T > 5$ GeV	100%
Overall		91.3%

Table 12 Cuts applied for B^+ selection after K^+ reconstruction.

Sample	Untagged signal	Untagged background	Lepton tagged signal	Lepton tagged background	B–π tagged signal	B–π tagged background
$B^+ \to J/\psi(\mu 6 \mu 3)K^+$	5,078,000	258,000	198,000	13,800	4,026,000	232,000
$B^+ \to J/\psi(\mu 6 \mu 5)K^+$	2,471,000	123,000	122,000	8,500	1,968,000	109,000
$B^0_d \to J/\psi(\mu 6 \mu 3)K^{*0}$	2,631,000	608,000	115,000	24,400	2,076,000	555,000
$B^0_d \to J/\psi(\mu 6 \mu 5)K^{*0}$	1,292,000	311,000	63,600	12,200	1,030,000	284,000

Table 13 Total number of events expected in the control samples (30 fb^{-1}). The B–π tagged events do not include the lepton tagged events.

tal background) is flat over the whole mass range (5-5.5 GeV) and contains vertices made of a true J/ψ combined with a true pion which in most of the cases (99%) do not come from a common decay $B^+ \to J/\psi\pi^+X$. The second component (57% of the total background) builds up the bump at low invariant masses and contains true J/ψ and true kaons, 12% of which coming from true $B^+ \to J/\psi K^+X$ decays. The third component (12% of the total background) is flat and includes all other topologies of events contributing to the background.

Also shown in Table 13 are the numbers of tagged events and respective backgrounds, both for lepton tagging and B–π tagging. As in the $B^0_d \to J/\psi(\mu\mu)K^0_s$ analysis, both muons and electrons with $p_T > 5$ GeV are used for tagging. A complete study of B–π tagging has not been performed for these channels, and tagging efficiencies on both signal and background equal to those estimated for the $B^0_d \to J/\psi(\mu\mu)K^0_s$ case have been used. In Table 13, lepton tagged events have been removed from the B–π tagged events.

8.1.2 Reconstruction of $B^0_d \to J/\psi(\mu\mu)K^{*0}$

Triggering of the $B^0_d \to J/\psi(\mu\mu)K^{*0}(K^+\pi^-)$ channel and J/ψ reconstruction were the same as for the $J/\psi(\mu\mu)K^+$ analysis. After the J/ψ was successfully reconstructed, all oppositely charged track pairs with $p_T > 0.5$ GeV were fitted to a common vertex and cuts given in Table 14 were applied. The value of σ is large (30 MeV) because of the significant contribution coming from the natural width (21 MeV). In the fit, both pion and kaon mass assignments were tried. If both combinations passed all the K^{*0} selection cuts, only the combination yielding the mass closest

to the nominal K^{*0} mass was retained.

The two muons and the two hadron tracks were then fitted to a common vertex. Due to the large K^{*0} width, a mass constraint was applied only to the J/ψ vertex. The final cuts on the B vertex were similar to those described for the $J/\psi(\mu\mu)K^{+}$ analysis and are summarized in Table 15, together with their relative efficiencies.

The mass peak is shown in Figure 14; the mass resolution is about 22 MeV. The number of expected signal events for an integrated luminosity of 30 fb^{-1} is shown in Table 13. The signal peak contains both the resonant decay (with the π and K masses assigned correctly in the K^{*0} fit) and the nonresonant process $B_d^0 \to J/\psi K\pi$ which accounts for 10% of the peak. The background includes the contribution from the reflection of the signal (π and K masses wrongly assigned in the K^{*0} fit), the contribution from other $B \to J/\psi X$ final states and purely combinatorial vertices. The main contributions to the $B \to J/\psi X$ part of the background are shown in Figure 15. The largest contribution is given by vertices made of a true J/ψ and two tracks not originating from the same vertex as the J/ψ [plot (a) in Figure 15]. Three contributions can be identified as coming

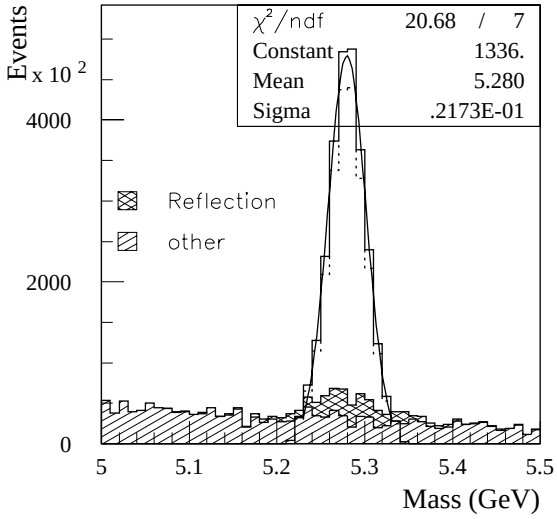

Figure 14 Invariant-mass distribution of the decay $B_d^0 \to J/\psi(\mu 6\mu 3)K^{*0}$ (open histogram) with superimposed the estimated background contribution (shaded histograms). The dotted line histogram shows the resonant component $B_d^0 \to J/\psi(\mu\mu)K^{*0}$ while the solid line histogram (the fitted one) also contains the contribution from nonresonant decays $B_d^0 \to J/\psi(\mu\mu)K\pi$.

Variable	Cut	Efficiency
Pair fit quality	χ^2 / d.o.f. < 6	75.4%
Mass window	[-3σ,+3σ] σ = 30 MeV	92.4%
K^{*0} transverse momentum	p_T > 3 GeV	77.3%
Overall		53.8%

Table 14 Cuts applied for K^{*0} selection after J/ψ reconstruction.

Variable	Cut	Efficiency
Successful kinematic fit	loose χ^2	99.8%
Mass window in barrel ($\|\eta\|$ < 0.7) in end-caps ($\|\eta\|$ > 0.7)	[-3σ,+3σ] σ = 16 MeV σ = 21 MeV	93.8%
Fit quality	χ^2 / d.o.f. < 6	99.6%
Transverse momentum	p_T > 5 GeV	100%
Overall		93.2%

Table 15 Cuts applied for B_d^0 selection after K^{*0} reconstruction.

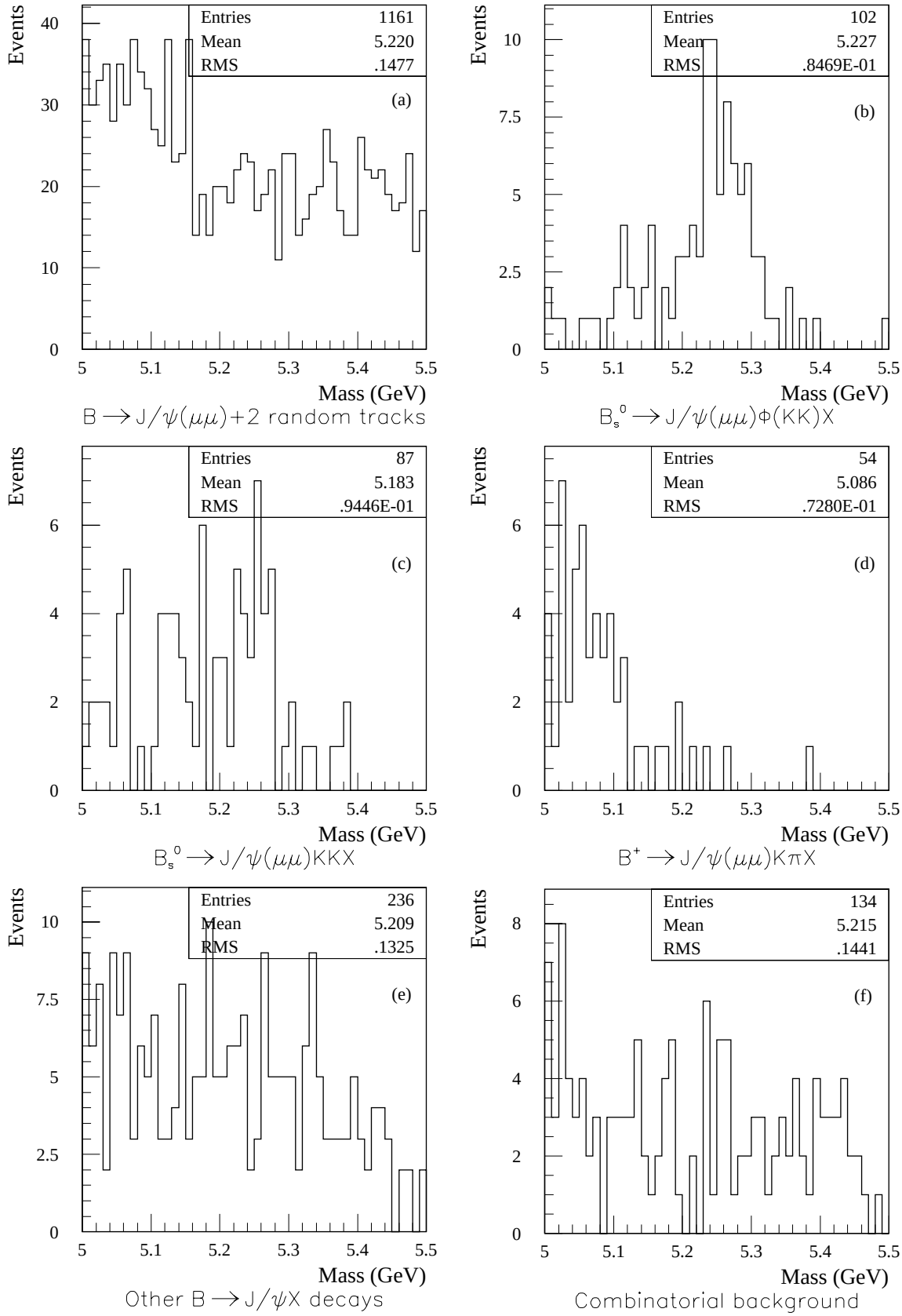

Figure 15 Contributions to the background of the $B_d^0 \to J/\psi K^{*0}$ decay channel, excluding the background coming from the reflection of the signal itself (see text for explanations).

from true B decays: $B_s^0 \to J/\psi(\mu\mu)\phi(KK)X$ decays (mainly contributing under the signal mass peak), $B_s^0 \to J/\psi(\mu\mu)KKX$ decays and $B^+ \to J/\psi(\mu\mu)K\pi X$ decays, increasing the background on the low mass side [plots (b), (c) and (d) in Figure 15]. The symbol "X" in these decays means that the partial Monte Carlo information available did not allow to exclude the presence of other particles coming from the same B vertex in the decay chain. The shape of the background coming from all other $B \to J/\psi X$ decays is shown in plot (e) and the purely combinatorial background is shown in plot (f) of Figure 15. Note that the peak in the background distribution (Figure 14) at the B_d^0 mass is due to the K^{*0} reflection, which represents 41% of the background under the peak while it accounts only for 6% of the background outside the peak over the mass range 5-5.5 GeV.

The numbers of tagged events (using lepton tagging and B–π tagging) and the respective numbers of background events are also shown in Table 13, after correction for the relevant efficiencies listed in Tables 4 and 8. The signal and background B–π tagging efficiencies have been deduced from the results obtained in the $B_d^0 \to J/\psi(\mu\mu)K_S^0$, as a complete study of the algorithm for this sample has not been performed yet.

8.2 Uncertainty on the production asymmetry

The production asymmetry, A^P, is not expected to exceed about 1% and it can be measured by using decay channels discussed above which are expected to have negligible CP violation. It can be measured in the untagged control samples by counting the numbers of reconstructed B and $\bar{B}$ mesons, taking into account the flavour oscillations in case of B_d^0 mesons. It is estimated that the statistical uncertainty on this measurement will be $\delta A^P = 0.05\%$ (0.07%) using the $B^+ \to J/\psi(\mu\mu)K^+$ sample and about 0.07% (0.10%) using the $B_d^0 \to J/\psi(\mu\mu)K^{*0}$ sample, for a LVL2 trigger muon threshold of 3 GeV (5 GeV) (see summary in Table 16). These estimates assume that any CP-violation effects in the two control samples can be neglected. The large number of events available in these channels should be sufficient to study the p_T dependence of any observed production asymmetry. However, this study has not been performed yet.

Systematic effects due to small differences in the reconstruction efficiencies for K^+ and K^- remain to be evaluated. A cross-check of corrections for such effects may be made by using the flavour oscillations in the decays $B_d^0 \to J/\psi(\mu\mu)K^{*0}$, for example.

8.3 Uncertainties from tagging

Systematic effects on the CP-violation asymmetry measurement related to tagging can be studied using the $B^+ \to J/\psi(\mu\mu)K^+$ and $B_d^0 \to J/\psi(\mu\mu)K^{*0}$ events, both for lepton (electron and muon) tagging and for B–π tagging (and for jet charge tagging which however will not be discussed here).

In all tagging methods, a fraction of the produced B mesons are mistagged, as discussed in Section 4. The wrong-tag fraction can be measured by comparing the numbers of positive-charge and negative-charge tags associated with the decays $B^+ \to J/\psi(\mu\mu)K^+$ and $B_d^0 \to J/\psi(\mu\mu)K^{*0}$, allowing for the oscillations in the case of B_d^0. The wrong-tag fraction can be measured separately for the tagging of B and $\bar{B}$ mesons, and the average value can be computed. By using the numbers of tagged signal and background events listed in Table 13, the statistical uncertainty on the measurement of the dilution due to tagging is estimated to be $\delta(D_{tag})/D_{tag} = 0.0038$ (0.0049) for lepton tagging using the $B^+ \to J/\psi(\mu\mu)K^+$ sample with a LVL2

trigger p_T threshold of 3 GeV (5 GeV) for the second muon. For B–π tagging the result is $\delta(D_{tag})/D_{tag}$ = 0.0030 (0.0040) for a 3 GeV (5 GeV) trigger threshold. Slightly larger uncertainties are obtained using the $B_d^0 \to J/\psi(\mu\mu)K^{*0}$ sample: $\delta(D_{tag})/D_{tag}$ = 0.0047 (0.0064) for lepton tagging and $\delta(D_{tag})/D_{tag}$ = 0.0039 (0.0050) for B–π tagging for a LVL2 trigger value of 3 GeV (5 GeV). All those figures are recalled in Table 16.

Asymmetries in the flavour-tagging algorithms can be due to trigger biases and asymmetries in the efficiency for reconstructing positively and negatively charged leptons and charged hadrons. The overall asymmetry in the tagging efficiency for B and $\bar{B}$ mesons can be measured using the $B^+ \to J/\psi(\mu\mu)K^+$ and $B_d^0 \to J/\psi(\mu\mu)K^{*0}$ events. It can be determined by counting the fraction of the events in the untagged B and $\bar{B}$ samples that contain a tag of either charge sign.

		$J/\psi(\mu 6\mu 3)K^+$	$J/\psi(\mu 6\mu 5)K^+$	$J/\psi(\mu 6\mu 3)K^{*0}$	$J/\psi(\mu 6\mu 5)K^{*0}$
δA^P		0.05%	0.07%	0.07%	0.10%
$\delta(D_{tag})/D_{tag}$	lepton tagging	0.0038	0.0049	0.0047	0.0064
$\delta(D_{tag})/D_{tag}$	B–π tagging	0.0030	0.0040	0.0039	0.0050

Table 16 Summary of the precision achievable on production asymmetry and tagging dilution using the two control channels described in the text (30 fb^{-1} of data).

8.4 Uncertainties from background

Another contribution to the systematic error on sin2β comes from the uncertainty on the backgrounds to the signal and to the control samples. Assuming a 5% (10%) uncertainty on the normalization of the background to the $B_d^0 \to J/\psi(\mu\mu)K_S^0$ decay, the uncertainty on the dilution from background is about $\delta(D_{back})/D_{back}$ = 0.006 (0.013) for the 3 GeV trigger threshold and $\delta(D_{back})/D_{back}$ = 0.006 (0.011) for the 5 GeV trigger option. The systematic uncertainty is smaller for the latter sample because the signal-to-background ratio is better with a 5 GeV cut on the second muon. Here it is assumed that there is no CP violation in the background.

9 Summary

Combining the various sources of uncertainty discussed in Sections 8.2, 8.3 and 8.4, one obtains an overall systematic error which is reported in Table 17 as a function of the background uncertainty and of the LVL2 muon trigger threshold.

Background uncertainty	$J/\psi(\mu 6\mu 3)K^+$	$J/\psi(\mu 6\mu 5)K^+$	$J/\psi(\mu 6\mu 3)K^{*0}$	$J/\psi(\mu 6\mu 5)K^{*0}$
5%	0.005	0.005	0.005	0.006
10%	0.008	0.008	0.009	0.008

Table 17 Systematic uncertainty on sin2β measurement as a function of background uncertainty and LVL2 muon trigger threshold after three years of running at low luminosity at the LHC (30 fb^{-1}).

In the best case (5% background uncertainty) the systematic error is independent of the trigger threshold and amounts to 0.005. The results are summarized for the whole period at low lumi-

nosity running (30 fb^{-1}) in Table 18.

LVL2 μ trigger	δ(sin2β) (statistics)	δ(sin2β) (systematics)
5 GeV	0.012	0.005
3 GeV	0.010	0.005

Table 18 Summary of the expected statistical and systematic uncertainties on sin2β after three years of running at low luminosity at the LHC (30 fb^{-1}).

10 References

[1] ATLAS Collaboration, Detector and Physics Performance: Technical Design Report 2, CERN / LHCC / 99-15 (1999).

[2] I. Gavrilenko, 'Description of Global Pattern Recognition Program (xKalman)', ATLAS Internal Note ATL-INDET-97-165 (1997).

[3] J. Damet and F. Tartarelli, 'K_S^0 reconstruction in the ATLAS Inner Detector', ATLAS Internal Note ATL-COM-INDET-99-021 (1999).

[4] ATLAS Collaboration, Detector and Physics Performance: Technical Design Report 1, CERN / LHCC / 99-14 (1999).

[5] F. Abe *et al.* (The CDF Collaboration), Phys. Rev. **D 59**, 32001 (1998).

[6] M. Gronau, A. Nippe and J. L. Rosner, Phys. Rev. **D47**, 1988 (1993).

[7] Private communication B. Bloch-Devaux (ALEPH database setup Nref 4).

[8] M. Smizanska *et al.*, 'Overview of simulations for ATLAS B-physics studies in period 1996-1999', ATLAS Internal Note ATL-COM-PHYS-99-042 (1999).

[9] E. J. Buis *et al.*, 'Update of Inner Detector performance parametrizations', ATLAS Internal Note ATL-INDET-98-215 (1998).

[10] ATLAS Collaboration, Technical Proposal, CERN / LHCC / 94-43 (1994).